








## An Approach for Volume Decomposition in Robot-Based Additive Manufacturing

Jacopo Lettori<sup>1,3</sup> , Roberto Raffaeli<sup>2</sup> , Milton Borsato<sup>3</sup> , Marcello Pellicciari<sup>2</sup>  and Margherita Peruzzini<sup>1</sup> 

<sup>1</sup>InterMech-DIEF, University of Modena and Reggio Emilia, [jacopo.lettori@unimore.it](mailto:jacopo.lettori@unimore.it), [margherita.peruzzini@unimore.it](mailto:margherita.peruzzini@unimore.it)

<sup>2</sup>InterMech-DISMI, University of Modena and Reggio Emilia, [roberto.raffaeli@unimore.it](mailto:roberto.raffaeli@unimore.it), [marcello.pellicciari@unimore.it](mailto:marcello.pellicciari@unimore.it)

<sup>3</sup> Universidade Tecnológica Federal do Paraná, [jacopo.lettori@unimore.it](mailto:jacopo.lettori@unimore.it), [borsato@utfpr.edu.br](mailto:borsato@utfpr.edu.br)

Corresponding author: Jacopo Lettori, [jacopo.lettori@unimore.it](mailto:jacopo.lettori@unimore.it)

**Abstract.** Robot-Based Additive Manufacturing (RBAM) combines material deposition nozzles and robotic manipulators to increase the flexibility of cartesian/delta Additive Manufacturing (AM) systems. RBAM overcomes the traditional limit given by the planarity of the manufacturing layer and allows variable slice thickness to be realized. Also, RBAM enables the deposition of the material in multiple directions. In this context, volume decomposition algorithms are implemented to split a solid into several sub-volumes. Each sub-volume is sliced according to an optimal direction to perform support-free manufacturing and to avoid tool collisions. A novel algorithm for the volume decomposition of a given input geometry is presented. In particular, it allows several planar separation surfaces to be computed that are used to split a general input shape. The surfaces are defined by analyzing overhangs according to an initial slicing direction. The normal of the surfaces identifies the slicing direction of the related sub-volumes. The algorithm steps are iterated to reach the complete removal of overhangs. The approach is tested in some case studies to evaluate its applicability.

**Keywords:** Volume decomposition; Additive Manufacturing; Robot-based Additive Manufacturing; Multi-Slicing Direction.

**DOI:** <https://doi.org/10.14733/cadaps.2023.1110-1127>

### 1 INTRODUCTION

Additive Manufacturing (AM) can be implemented with robotic manipulators [19] to increase the flexibility of cartesian/delta AM. Also, researchers have used work tables with certain degrees of freedom [12] for the same aim. Direct Energy Deposition (DED) [9] is one of the solutions for Robot-Based Additive Manufacturing (RBAM), where the material is deposited from a nozzle onto support [1]. The raw material can be in wire or powder form. Recently, Wire and Arc Additive

Manufacturing (WAAM), a form of wire-based DED process, is also gaining interest from both academic and industrial points of view. WAAM is an automated welding process where parts are manufactured thanks to a welding gun moved by a manipulator according to 3D paths [22]. The main advantages of WAAM are flexibility, low capital investment, and low material cost [23]. Similarly, extruders for polymeric materials are used in RBAM. Furthermore, RBAM can be integrated with chip removal solutions to improve the quality and surface finishing of the product [17].

In particular, RBAM allows the deposition of material in multiple directions [27] thanks to the flexibility of manipulators. Indeed, RBAM overcomes the traditional limit given by the planarity of the manufacturing layer and allows variable slice thickness to be realized. To maximize deposition freedom, part geometry needs to be decomposed into sub-volumes. Then, a suitable slicing strategy is defined for each sub-volume to minimize and possibly remove the need for supports [13], leveraging the possibility of changing the deposition direction. However, software tools to support this approach are not widespread. Commercial systems such as Netfabb, 3DS, and Cura target delta/cartesian AM, and the slicing direction is the only allowed option. Specialized software for WAAM exist, such as WAAM3D [31]. However, their use is still limited. Tools for the volume subdivision are lacking, which is a mandatory step for multi-direction deposition. Therefore, ad-hoc manual procedures are used to decompose the volume and calculate layers and paths.

In this context, this paper presents an algorithm for volume decomposition based on the input geometry. It has been developed for planar slicing and layers with constant thickness. The algorithm finds planar separation surfaces used to split the initial volume into a certain number of sub-volumes to remove the need for support.

The remainder of the paper is organized as follows. The state of the art of volume decomposition algorithms is reported in section 2. The proposed approach is outlined in section 3. In section 4, the algorithm is applied to some case studies to show its robustness. Finally, conclusions and future works are presented in section 0.

## 2 STATE OF THE ART

Algorithms for volume decomposition can be found in the literature, such as the Chopper algorithm [9]. This algorithm was developed for cartesian/delta printers, and it computes planar separation surfaces to divide an input geometry given the limitations of printers' build volume, as shown in Figure 1a. Each sub-volume is assembled after the manufacturing phase, thanks to correctly designed connectors. However, this algorithm does not include minimization of the overhangs.

Starting from an initial slicing direction, the silhouette curve algorithm [16] divides the initial geometry into a certain number of sub-volumes by evaluating the surface normal at each point. Silhouette curves are used to split the volume into buildable and unbuildable parts when an overhang is identified (see Figure 1b). This algorithm was developed for RBAM even if some geometries cannot be handled appropriately.

Similarly, several cutting planes algorithms [3,4,11,25,28] aim at dividing an input geometry into sub-volumes to remove the need for supports using cutting planes. The planes are computed by analyzing the overhang areas according to an initial slicing direction (SD). Usually, the normal of the planes are the SDs of the related sub-volumes, as shown in Figure 1c. Greedy algorithms [11] define the required cutting planes to remove the overhangs and avoid tool collisions. However, the created subdivisions could be non-optimal and leave overhangs, or many sub-volumes can be generated. Heuristics have been defined [3] to improve the volume decomposition, even if the user is required to define the desired number of cutting planes.

On the other hand, the algorithm proposed in [25] computes the buildable regions, the unbuildable regions, and the intersecting geometry curve according to an initial slicing direction. Decomposing surfaces are computed by parametrizing overhang surfaces and evaluating their directional profiles. Also, the algorithm provides a build sequence without tool collision. However,

this algorithm generates a large number of sub-volumes. Finally, the cusp-height minimization algorithm [28] is implemented to compute cutting planes. However, this method is mainly suited for tree-like structures.

Similarly, the beam-guided searching algorithm [24] determines the volume decomposition in terms of a sequence of clipping planes. The normal to the planes are the slicing directions of the sub-volumes. In this case, beam-guided search is implemented to improve the outputs of an initial constrained greedy scheme, providing a possible optimum decomposition. In particular, this algorithm stores a list of clipping planes in each beam. The clipping planes are computed considering the maximization of the descent of overhang areas while imposing that these areas are self-supported.

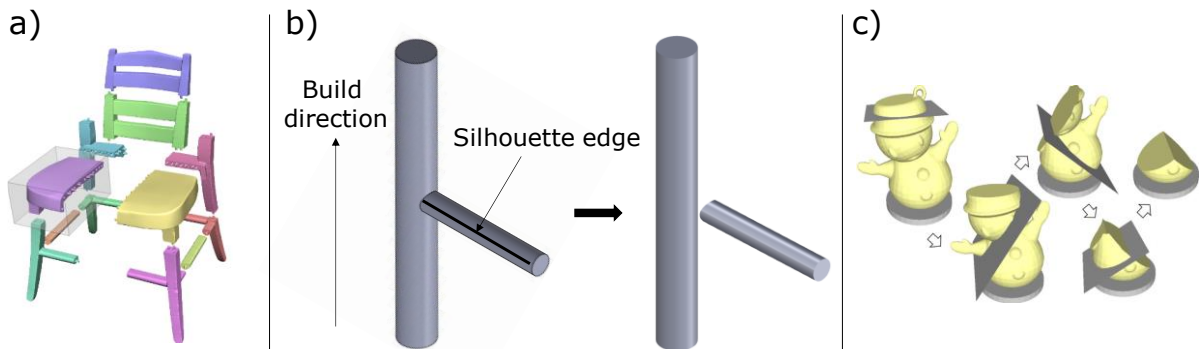


**Figure 1:** a) Chopper algorithm, taken from [9]; b) Silhouette algorithm, adapted from [16]; c) Cutting planes algorithm, taken from [24].

The concave loop extraction algorithm [2,13] is another practical approach for volume decomposition. A series of connected concave edges give a concave loop, and these loops divide the part surface in connected regions and the whole solid into sub-volumes [30]. A reference slicing direction is then calculated using the Minimal Enclosing Crown (MEC) algorithm [29]. This method depends on concave edges or a fixed curvature threshold used to find concave loops. Therefore, some sub-volumes may be missed, especially in the presence of non-trivial geometries.

On the other hand, the curve skeleton-based algorithm [20,21] uses the 1D medial axis [5,18] of input geometry to decompose the volume and find the slicing direction. However, the medial axis is mainly suited for tree-like geometries. Also, the accuracy of the medial axis depends on the quality of the mesh [20].

Some cases in which the described algorithms have been applied are depicted in Figure 2.

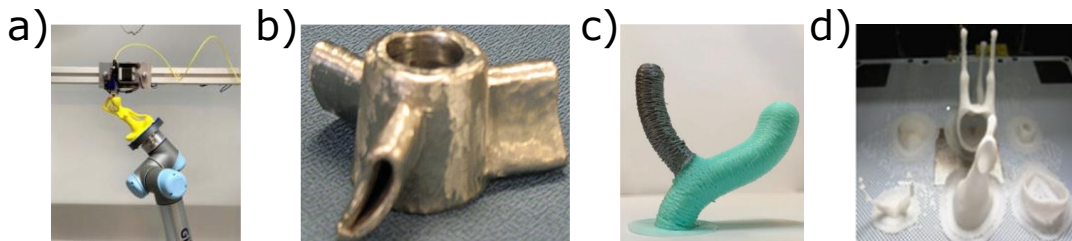


**Figure 2:** Test cases from the reviewed papers: a) taken from [24]; b) taken from [13]; c) taken from [20]; d) taken from [21].

The mentioned algorithms look for discrete numbers of sub-volumes and compute a slicing direction for each of them. On the other hand, RBAM can continuously change the deposition

direction to perform a continuous deposition. Centroidal axis extraction [14], medial axis [6,26], or surface extraction [7] algorithms are used in this case. However, these algorithm presents the same limits as the curve skeleton-based algorithm. In particular, the medial axis is mainly suited for tree-like geometries, and its accuracy may depend on the quality of the input mesh.

The reviewed methods are not suited for all types of geometries, and many sub-volumes are often computed. Also, few algorithms have been applied to industrial parts. So, this paper presents an algorithm to perform support-free RBAM to cope with the elaboration of generic geometries, generating sub-volumes only where necessary. Also, the algorithm has been tested in few case studies, also from the industrial field.

**3 PROPOSED ALGORITHM**

The proposed approach for volume decomposition is a part of a framework to accomplish and optimize RBAM, which can be found in [5]. The overall algorithm is depicted in Figure 3.

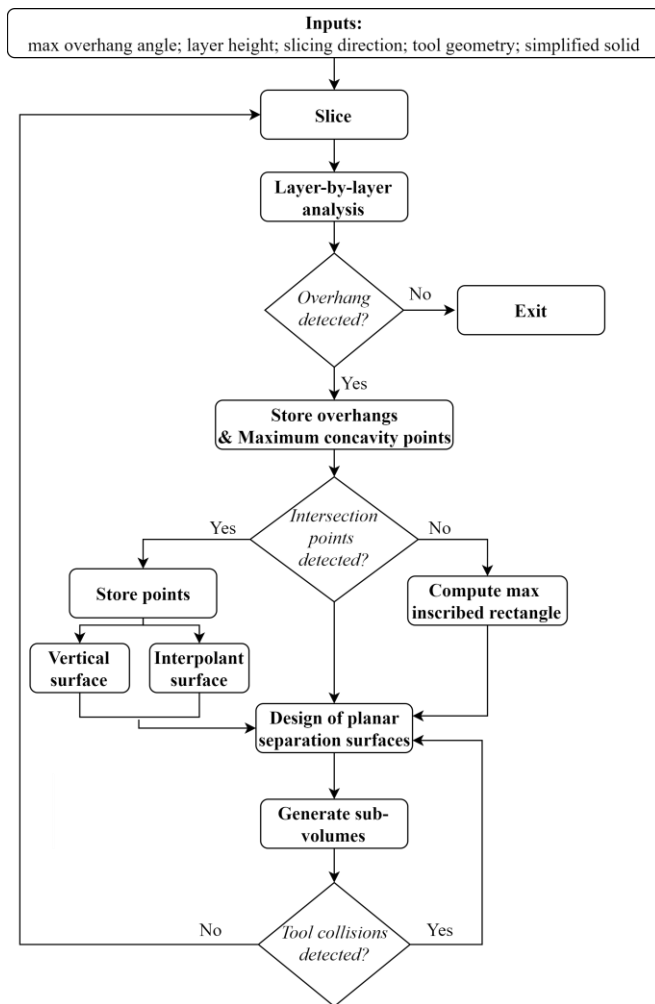


**Figure 3:** Overall algorithm flowchart for RBAM volume subdivision.

The input geometry is firstly simplified by removing holes and small features that are not intended to be realized by material deposition. Then, the whole volume is sliced according to an optimal direction chosen from an evaluation of the optimal orientation to support the part on the supporting base. Layer distance is given as a parameter according to the deposition technology. The slicing process defines a sequence of consecutive layers composed of the intersection of the sectioning planes with the volume boundary. Then, each layer is processed to identify overhangs as described in the following section 3.1. When overhangs are identified, a splitting process is triggered to divide the volume into portions manufactured separately. The approach provides planar separation surfaces whose normals are the slicing directions of the subsequent sub-volumes. The process is iterated until the overhangs are entirely removed.

### 3.1 Layer-by-layer Analysis

In this phase, the volume is analyzed layer-by-layer. Closed curves form each layer section, as shown in Figure 4. Inner holes are neglected for simplicity. The transition from one layer to the next one is iteratively analyzed. As well known, AM technologies require the deposited material to be supported by the previously added material. However, a specific prominence is allowable around the sliced contour. Experimental tests have shown that a maximum overhang angle can be assumed according to the selected technology and process parameters [16]. The maximum overhang angle is the value at which external supports are required if the slope of the part exceeds the value. This means that the supporting area provided by a previous layer can be determined by an offset of the layer curves toward the outer side (black solid curve) by an amount depending on the layer thickness and the maximum overhang angle. So, a layer  $l_i$  (black dashed curve) is offset. Then, the offset of  $l_i$  is projected onto the  $l_{i+1}$  plane (solid red curve). In this case, it is assumed an overhang angle of  $45^\circ$  and a layer thickness of 3mm.

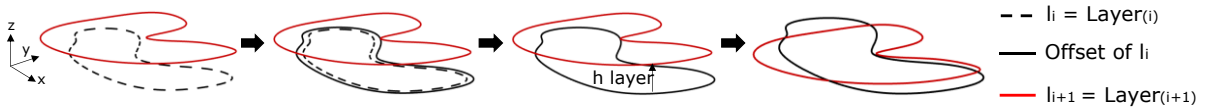


Figure 4: Layer-by-layer analysis.

Three scenarios can occur when two consecutive layers are analyzed, as depicted in Figure 5.

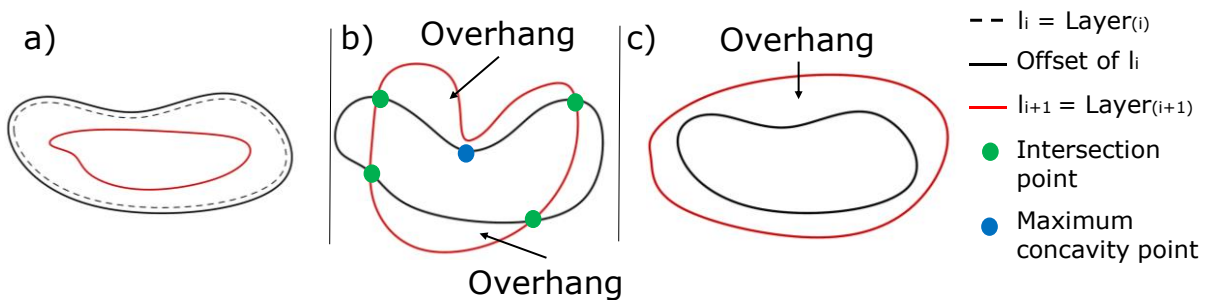
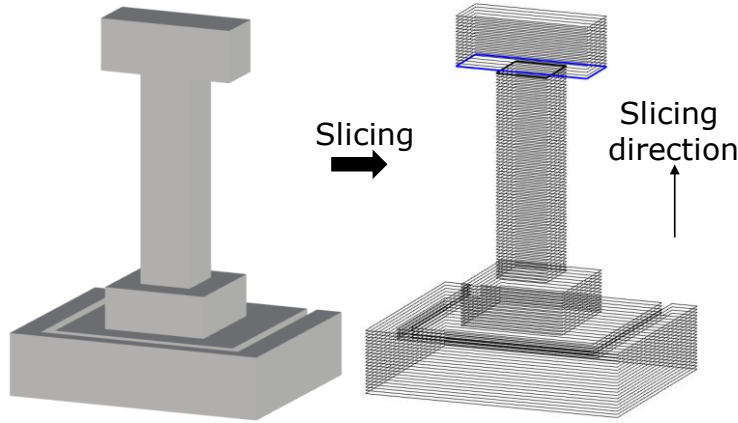


Figure 5: Scenarios when two consecutive layers are analyzed: a)  $l_{i+1}$  is entirely supported by  $l_i$ ; b)  $l_{i+1}$  is not entirely supported, and it intersects the offset of  $l_i$ ; c)  $l_{i+1}$  is not entirely supported, and it does not intersect the offset of  $l_i$ .

A simplified exemplary case is shown in Figure 6. The solid is analyzed layer by layer from the bottom to the top. Initially, each layer is fully supported by the previous one. When the slope of the lateral surface increases over a threshold angle, the algorithm encounters the scenario

depicted in Figure 5b. Four points are found from the intersection between the offset of  $l_i$  and  $l_{i+1}$  (Figure 7b). Thus,  $l_{i+1}$  consists of a supported area (bounded by the solid green curve) and two overhangs (bounded by the red solid curves), as shown in Figure 7c. The algorithm separates these three parts and stores the intersection points. Also, the algorithm identifies maximum concavity points by analyzing the curvature of the intersection curve, as depicted in Figure 5b. Such points are encountered when the curvature is concave and assumes a maximum relative value. Note that the algorithm clusters the intersection points and maximum concavity points and treats the two overhangs as separate entities. Finally, it generates the offset of the supported area, as shown in Figure 7d. This offset is projected onto the next layer, defining the supported area. The algorithm iterates the steps until the last layer.



**Figure 6:** Example of volume slicing: on the right, the case of an unsupported layer is highlighted.

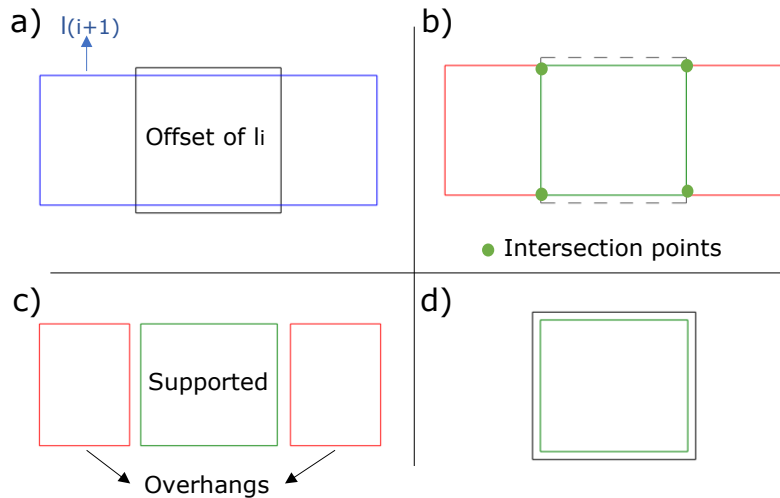


**Figure 7:** Layer processing steps: a) The offset of  $l_i$  is projected onto  $l_{i+1}$ ; b) Identification of intersection points; c) Separation of overhangs and supported area of  $l_{i+1}$ ; d) Offset of the supported area of  $l_{i+1}$  (black solid curve).

At the end of the process, the algorithm has identified the supported layers (green curves), unsupported layers (red curves) and the intersections points, as shown in Figure 8.

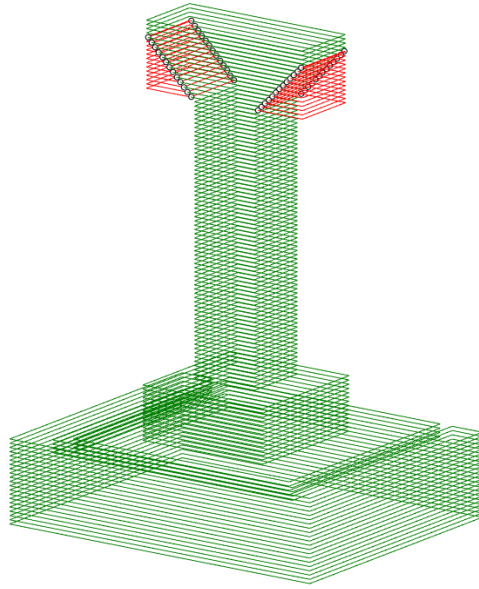


**Figure 8:** Layer-by-layer analysis and intersection points identification.

### 3.2 Definition of the Planar Separation Surfaces

From the output of the previous step, planar separation surfaces are calculated to remove from the volume a portion to be deposited in another direction. As a first step, the algorithm computes an interpolant plane of the intersection points, as shown in Figure 9. The interpolation is computed as a standard minimization of distances between the plane and the intersection points.

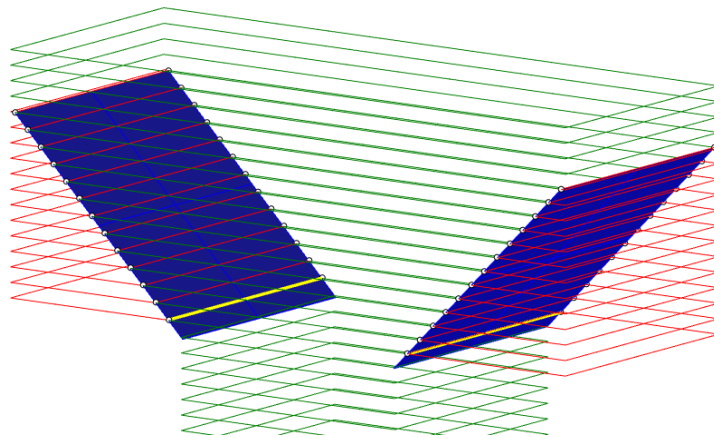


**Figure 9:** Interpolant surfaces. The yellow lines obtained as the intersection with the plane of the first layer with overhangs are used as rotation axes.

The algorithm generates the intersection between the interpolant surfaces and the first layer containing an overhang, identifying the line marked in yellow in Figure 9. Then, two possible options can be selected as described in the two following paragraphs, i.e., the interpolant separation surface and the vertical separation surface.

### 3.2.1 First option: interpolant separation surface

Due to the interpolation process, the slope of the resulting separation surface may slightly exceed the maximum allowable overhang angle. In this case, the slope is reduced to comply with the maximum allowable overhang, increasing the  $\lambda$  angle (Figure 10a). The surface is rotated around the yellow line depicted in Figure 9, given by the intersection with the plane of the first layer with overhangs. Then, the planar surface is translated along its normal to leave all the intersections and maximum concavity points aside. This surface is used to build the subdivision surface.

The extension of the separation surface is limited to the layers with overhang portions. Therefore, additional tilted surfaces guarantee a complete intersection with the initial volume, as shown in Figure 10b. The slope of the surfaces is required to avoid collisions between the extruder/torch and the already deposited material, as further described in section 3.2.4. Therefore, the final separation surfaces are formed by the interpolant separation surfaces (blue surfaces), whose normal is the slicing direction of the related sub-volume, and a variable number of tilted separation surfaces (grey surfaces), as depicted in Figure 10c.

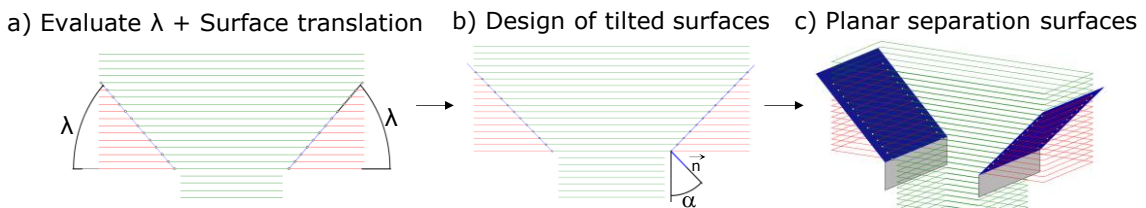


**Figure 10:** Development of cutting surfaces: first option.

Three sub-volumes are obtained from the adopted case, as depicted in Figure 11.

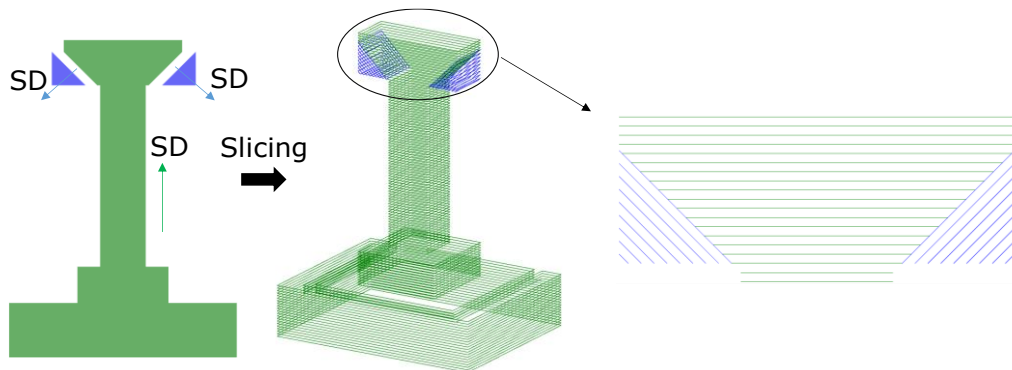


**Figure 11:** Sub-volumes obtained through the interpolant separation surface option.

### 3.2.2 Second option: vertical separation surface

A vertical surface passing through the rotation axis (yellow line depicted in Figure 9 and Figure 12a) is used as a subdivision surface. The surface is then translated to touch the intersection points or maximum concavity points (Figure 12b). The normal of this surface is orthogonal to the current slicing direction. Also, in this case, tilted surfaces are added. Note that tilted surfaces are translated along the separation surface if they do not intersect any intersection point or the curve that forms the overhang. Again, the final planar separation surfaces are formed by the vertical separation surfaces (blue surfaces), whose normal is the slicing direction of the related sub-volume and the tilted separation surfaces (grey surfaces), as depicted in Figure 12c.



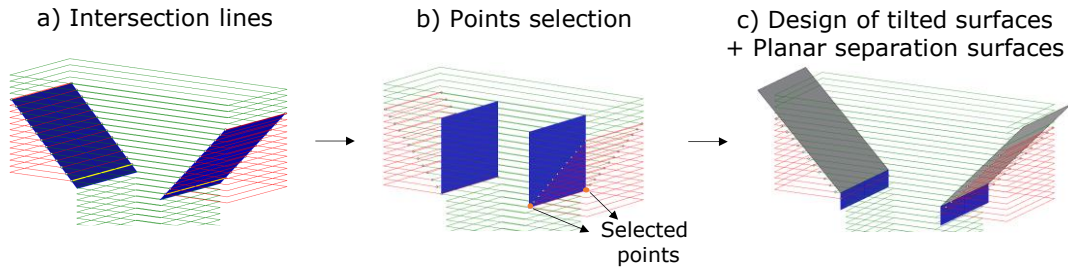


**Figure 12:**Development of planar separation surfaces: the second option.

Three sub-volumes are obtained through this method, as depicted in Figure 13.

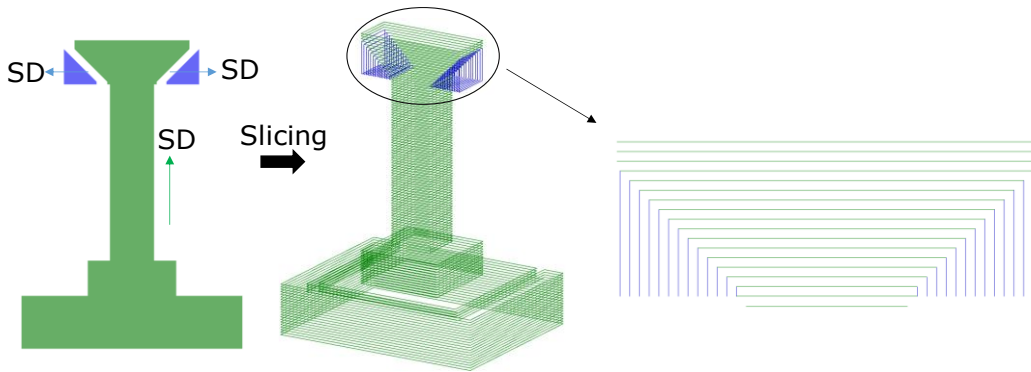


**Figure 13:** Sub-volumes obtained through the vertical separation surface approach.

3.2.3 Maximum axis-aligned rectangle inscribed in the layer curve

When the scenario in Figure 5c occurs, no intersection points are found. The Maximum Axis-Aligned Rectangle Inscribed on a Curve (MAARIC) algorithm [10] is used to define four planar separation surfaces, as shown in Figure 14a. The normal of the four surfaces are perpendicular to the original slicing direction (Figure 14b) and represent the direction of four distinct volume portions to be manufactured. Thus, the rectangle corresponds to the supported and buildable part of the layer. The remaining four-volume portions are deposited in inverse order, i.e., from 4 to 1, to avoid collisions with already deposited material.

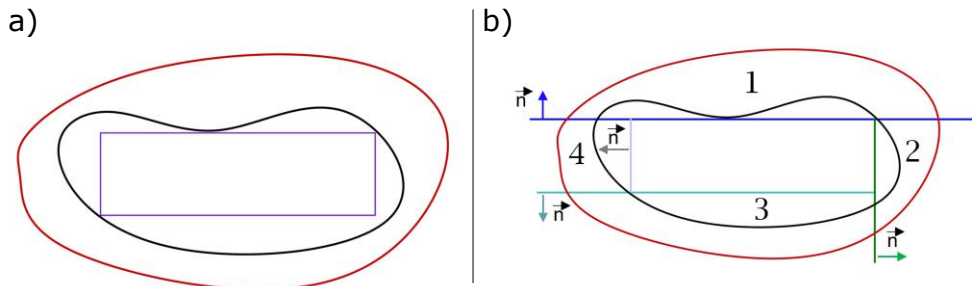


**Figure 14:** a) MAARIC algorithm result using the supported layer curve [10]; b) Planar separation surfaces generated based on the maximum inscribed rectangle.

The method related to the first encountered scenario is applied if the part presents both scenarios of Figure 5b and Figure 5c. The volume subdivision process is iteratively applied, finding new sub-volumes and new slicing directions until all the overhang portions are eliminated.

3.2.4 Tilted surfaces definition

As introduced in section 3.2.1, the extension of the separation surface is limited to the layer with overhang portions. Therefore, additional tilted surfaces must guarantee a complete intersection with the processed volume to provide the generation of sub-volumes. The slope of the tilted surfaces is required to avoid collisions between the extruder/torch and the already deposited material. In particular, the encumbrance of the deposition head is identified with the angle  $\beta$ . It depends on the geometric characteristics of the extruder/torch, such as the diameter, and the distance between the tool head and the substrate, as shown in Figure 15. So, the angle  $\alpha$  between the normal of the separation surface and the tilted surface must be equal to or greater than angle  $\beta$  to guarantee tool accessibility. Indeed, collisions between the torch/extruder and the deposited material occur if angle  $\alpha$  is below angle  $\beta$ . However, angle  $\alpha$  must also be compatible with the maximum overhang angle  $\theta$  when angle  $\beta$  is below  $(\pi/2 - \theta)$ . In this case, angle  $\alpha$  is equal to  $(\pi/2 - \theta)$  to avoid the generation of further overhangs, as depicted in Figure 15.

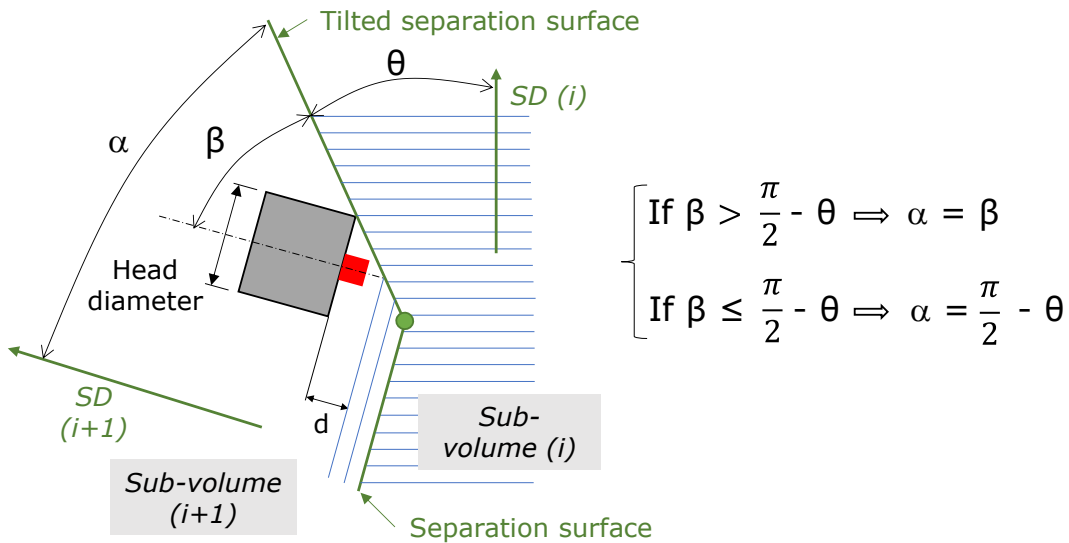


**Figure 15:** Encumbrance of the deposition head and determination of the slope of the tilted separation surface. SD: Slicing direction;  $\alpha$ : angle between the normal of the separation surface and tilted separation surface;  $\beta$ : encumbrance of tool head;  $\theta$ : maximum overhang angle.

So, the tilted separation surface is required when the separation surface exceeds the extension of the overhang, as shown in Figure 16a. Finally, the tilted surface is translated to touch the intersection points or the overhang curve. However, the separation surface must extend for at least one layer to maintain the topology of the separation surfaces and provide the deposition head accessibility (see Figure 16c). This step is performed to avoid the removal of too large sub-volumes.

4 TESTING OF THE ALGORITHM

In this section, six case studies are presented to test the applicability of the proposed algorithm. The selected technology is WAAM. These test cases have been selected to verify the algorithm's

capability to process the geometry successfully. These test cases have been selected as they are suited for RBAM, especially considering WAAM [8].

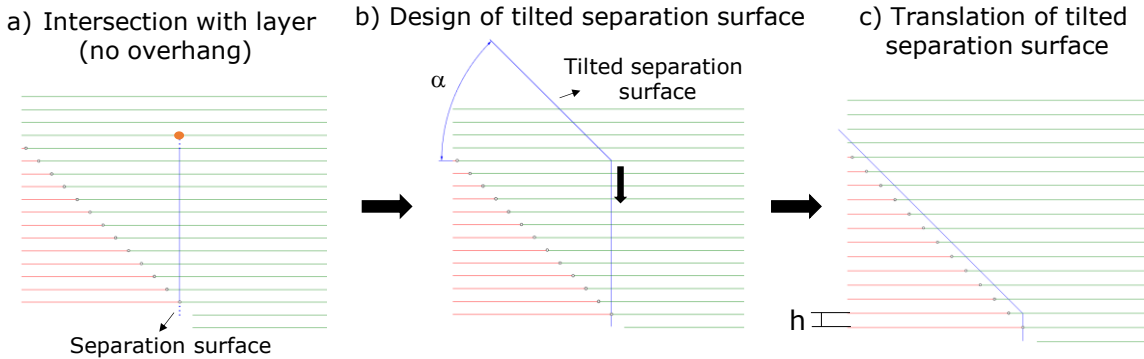


**Figure 16:** Definition of the tilted separation surfaces.

Also, some case studies are taken from the analyzed literature (see column Ref of Table 1). In these case studies, the holes are simplified as they can be realized most conveniently in the post-processing phase, except for the test case depicted in Figure 19. Table 1 summarizes the geometry characteristics of the initial volume, the input parameters, and the applied algorithm for each test case. Also, it highlights whether the algorithm successfully decomposes the geometry.

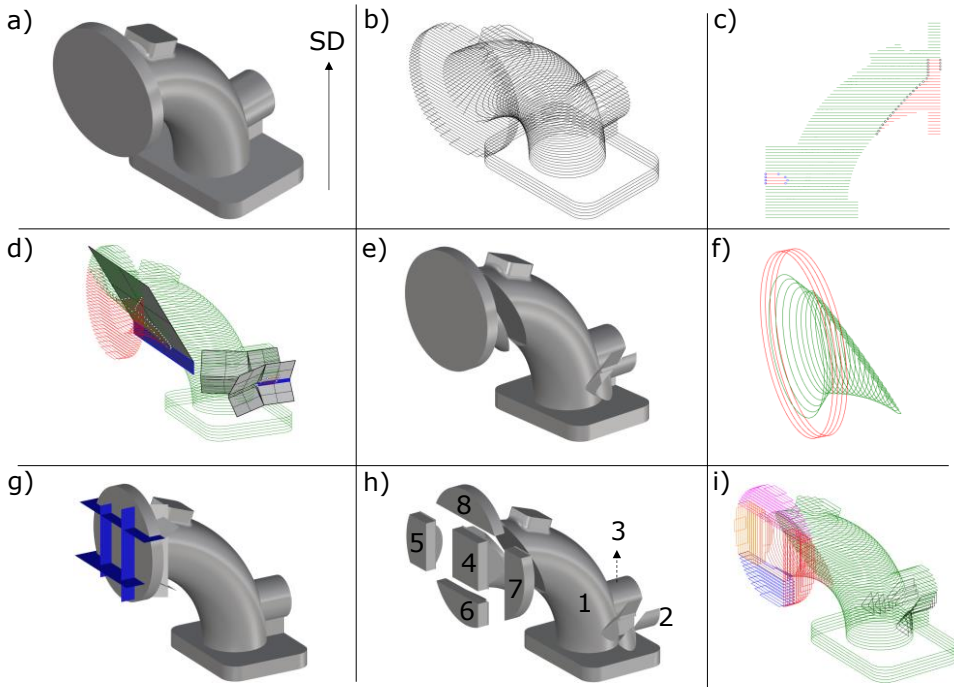
Test case	Figure	Size (mm)	S	LH (mm)	$\theta$	$\beta$	A	Success	N° SV	Ref
<b>Case 1</b>	Figure 17	170x120x190	Yes	3	45°	60°	V	OK	8	\
	Figure 18	170x120x190	Yes	3	45°	40°	I	OK	6	\
<b>Case 2</b>	Figure 19	170x120x190	No	3	45°	40°	V	OK	9	\
<b>Case 3</b>	Figure 20	400x200x260	Yes	3	45°	35°	V	OK	3	[4]
	Figure 21	400x200x260	Yes	3	45°	35°	I	OK	2	[4]
<b>Case 4</b>	Figure 22	200x370x365	Yes	3	45°	45°	V	OK	5	[2]
<b>Case 5</b>	Figure 23	130x180x194	Yes	3	45°	60°	I	OK	7	[5]
<b>Case 6</b>	Figure 24	335x367x100	Yes	3	37°	60°	I	OK	7	[29]

**Table 1:** Summary of the case studies and related parameters. Column S reports if the volume was simplified from holes and small features; LH: Layer Height;  $\theta$ : Overhang angle; A: implemented algorithm (option V: vertical separation surface; option I: interpolant separation surface); N° SV: number of sub-volumes.

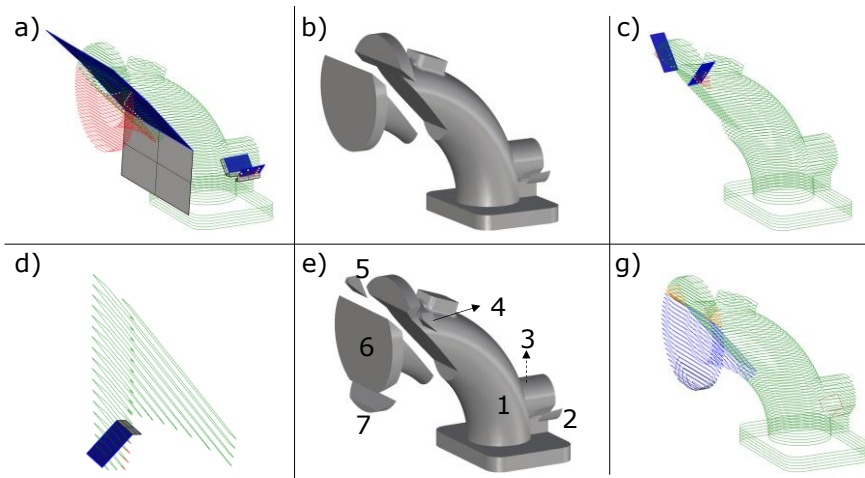
### 5 DISCUSSION

Table 2 summarizes the main features of the proposed approach compared to the main algorithms analyzed from the literature.

The proposed algorithm has successfully decomposed the presented test cases into sub-volumes and computed a slicing direction to perform support-free manufacturing. The results are not depending on the quality of the input mesh and the geometry and no space partitioning. Also, the proposed approach can elaborate geometries even in the cases where concave loops subdivision is not helpful. Finally, tilted separation surfaces are calculated that are essential to generate reasonable sub-volumes and avoid tool collisions.



**Figure 17:** First test case with vertical surface option: a) Initial volume; b) Slicing; c) Layer-by-layer analysis; d) Planar separation surfaces; e) Sub-volumes; f) Layer-by-layer analysis of the sub-volume; g) Planar separation surfaces of the sub-volume using MAARIC algorithm; h) Final sub-volumes and build order; i) Final slicing. The normal to the blue surfaces are the slicing directions of the related sub-volume.



**Figure 18:** First test case with interpolant surface option: a) Planar separation surfaces; b) Sub-volumes; c) Layer-by-layer analysis of the sub-volume 1 with planar separation surfaces; d) Layer-by-layer analysis of the sub-volume 2 with planar separation surface; e) Final sub-volumes and build order; g) Final slicing. The normal of the blue surfaces are the slicing directions of the related sub-volume.

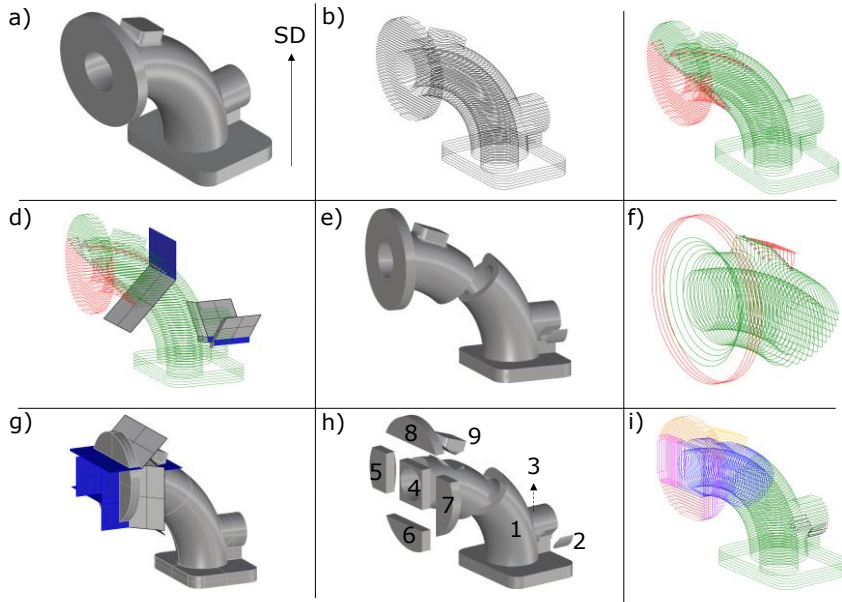


**Figure 19:** Second test case with vertical surface option: a) Initial volume; b) Slicing; c) Layer-by-layer analysis; d) Planar separation surfaces; e) Sub-volumes; f) Layer-by-layer analysis of the sub-volume; g) Planar separation surfaces of the sub-volume using MAARIC algorithm; h) Final sub-volumes and build order; i) Final slicing. SD: Slicing direction. The normal of the blue surfaces are the slicing directions of the related sub-volume.

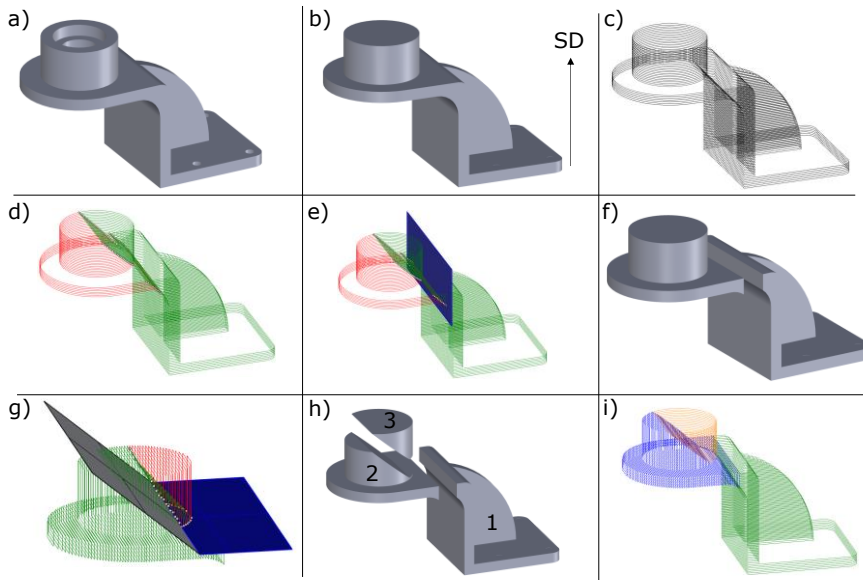


**Figure 20:** Third test case with vertical surface option: a) Initial volume; b) Simplified volume c) Slicing; d) Layer-by-layer analysis; e) Planar separation surfaces; f) Sub-volumes; g) Layer-by-layer analysis of the sub-volume and planar separation surface; h) Final sub-volumes and build order; i) Final slicing. SD: Slicing direction. The normal of the blue surfaces are the slicing directions of the related sub-volume.

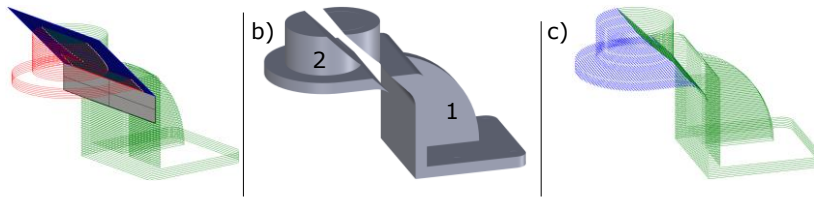


**Figure 21:** Third test case with interpolant surface option: a) Planar separation surfaces; b) Sub-volumes; b) Final sub-volumes and build order; c) Final slicing. The normal of the blue surfaces are the slicing directions of the related sub-volume.

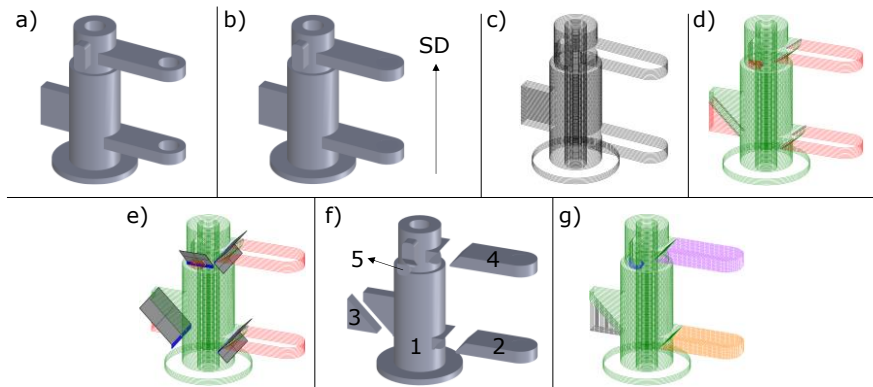


**Figure 22:** Fourth test case with vertical surface option: a) Initial volume; b) Simplified volume c) Slicing; d) Layer-by-layer analysis; e) Planar separation surfaces; f) Sub-volumes and build order; g) Final slicing. SD: Slicing direction. The normal of the blue surfaces are the slicing directions of the related sub-volume.

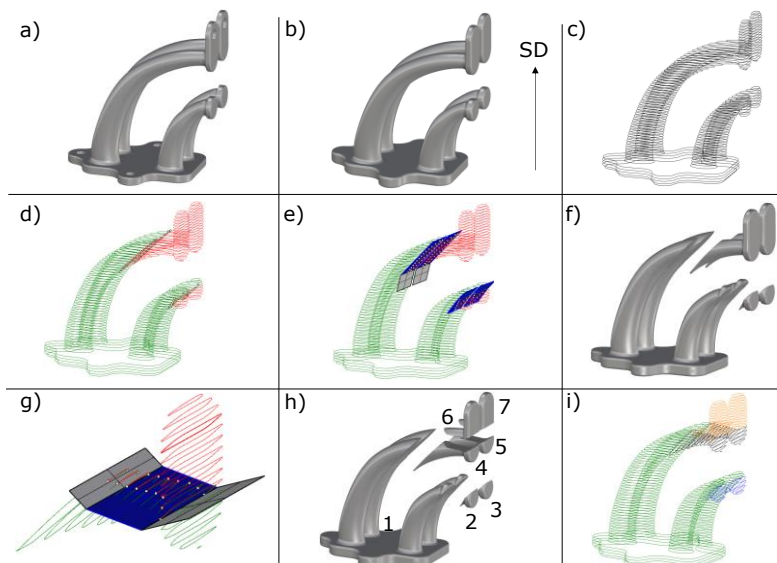


**Figure 23:** Fifth test case with the algorithm of the adaptation of interpolant surface: a) Initial volume; b) Simplified geometry; c) Slicing; d) Layer-by-layer analysis; e) Planar separation surfaces; f) Sub-volumes; g) Layer-by-layer analysis of the sub-volume with planar separation

surface; h) Final sub-volumes and build order; i) Final slicing. SD: Slicing direction. The normal of the blue surfaces are the slicing directions of the related sub-volume.

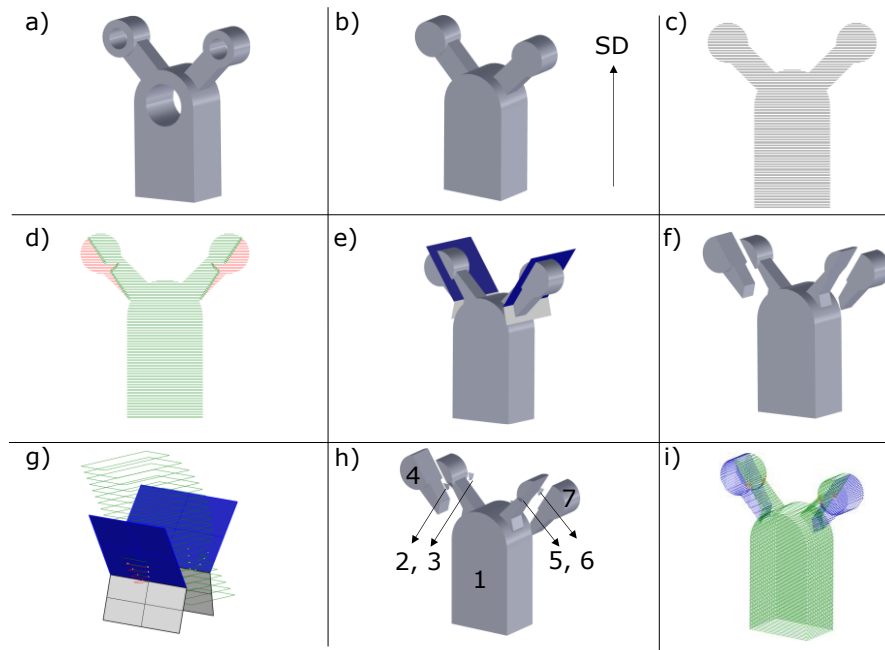


**Figure 24:** Sixth test case with the algorithm of the adaptation of interpolant surface: a) Initial volume; b) Simplified geometry; c) Slicing; d) Layer-by-layer analysis; e) Planar separation surfaces; f) Sub-volumes; g) Layer-by-layer analysis of the sub-volume with planar separation surface; h) Final sub-volumes and build order; i) Final slicing. SD: Slicing direction. The normal of the blue surfaces are the slicing directions of the related sub-volume.

However, the proposed algorithm presents some limits. Cavities whose principal extension is not parallel to the slicing direction should be simplified to increase the stability of the approach. The algorithm has generated small sub-volumes in few cases, as shown in Figure 18c and Figure 24g. These sub-volumes could be challenging to be manufactured. Finally, this algorithm is better suited for three-like structures and bulk geometries, while a different approach should be devised for thin structures.

Algorithm	Features								Geometry compatibility		
	MD	VD	CLD	OHO	NPR	SSV	TCE	TS	TLS	TG	BG
Proposed method	x	x	x	✓	x	✓	✓	✓	✓	x	✓
Beam-guided [24]	x	✓	x	✓	x	x	✓	x	x	x	✓
Skeleton-based [14,20,21]	✓	x	x	✓	✓	✓	x	x	✓	✓	x
Concave loop [2,13]	x	x	✓	✓	x	x	x	x	x	x	✓
Chopper [9]	x	x	x	x	x	x	x	x	✓	x	✓
Silhouette [16]	x	x	x	✓	x	✓	✓	x	x	x	✓
Cusp-height	x	x	x	✓	x	✓	✓	x	✓	x	x

Algorithm	Features								Geometry compatibility		
	MD	VD	CLD	OHO	NPR	SSV	TCE	TS	TLS	TG	BG
minimization [28]											
Cutting planes [3,4,11,25]	x	x	x	✓	x	x	✓	x	✓	x	✓

**Table 2:** Comparison among multi-axis deposition algorithm. Md: mesh dependency; vd: dimension of the voxel dependency; cld: concave loop dependency; oho: overhang optimization; npr: non-planar slicing recommended; ssv: generation of small sub-volumes; tce: tool collision evaluation; ts: generation of tilted separation surfaces; tls: tree-like structures; tg: thin geometry; bg: bulk geometry.

## 6 CONCLUSIONS & FUTURE WORKS

This paper presents an algorithm for volume decomposition to perform multi-direction deposition in the RBAM context. The algorithm's objective is to limit and possibly remove the need for support due to overhangs. The proposed method provides several planar separation surfaces to split an initial volume into sub-volumes when overhangs are detected. Also, the algorithm checks tool accessibility, and it is iterative, guaranteeing support-free manufacturing if possible.

Planar separation surfaces are defined accordingly to the different cases encountered in the layers' succession. Since the planar separation surface extension is limited to the overhang area, the approach introduces tilted surfaces to properly separate volumes and avoid tool head collision while depositing the following sub-volumes. So, the final planar separation surface is composed of a separation surface whose normal is the slicing direction of the related sub-volume and tilted separation surfaces to guarantee the subdivision.

The algorithm needs further testing to highlight critical issues in more complex parts as future work. Currently, the algorithm was developed considering planar slicing with constant thickness, and this represents a limit since the possibility of curved layers with non-uniform thickness provided by RBAM is not exploited. Several geometries would benefit from non-planar and non-uniform slicing. For example, the first, the second, and the fifth test cases are promising candidates for non-planar and non-uniform slicing as they present curved sub-volumes. So, an extension of the algorithm should be developed to apply the best type of slicing according to the geometry features. An extensive experimental campaign should be foreseen to assess the quality of the produced parts and optimize the required process parameters. Finally, the algorithm will be optimized in terms of output performances to obtain the best volume decomposition.

Jacopo Lettori, <https://orcid.org/0000-0002-8523-8469>

Roberto Raffaelli, <https://orcid.org/0000-0003-0301-454X>

Milton Borsato, <https://orcid.org/0000-0002-3607-8315>

Marcello Pellicciari, <https://orcid.org/0000-0003-2578-4123>

Margherita Peruzzini, <https://orcid.org/0000-0003-2260-0392>

## REFERENCES

- [1] Dass, A.; Moridi, A.: State of the Art in Directed Energy Deposition: From Additive Manufacturing to Materials Design, Coatings, 9(7), 2019, 418. <https://doi.org/10.3390/COATINGS9070418>.
- [2] Ding, D.; Pan, Z.; Cuiuri, D.; Li, H.; Larkin, N.; Van Duin, S.: Automatic Multi-Direction Slicing Algorithms for Wire Based Additive Manufacturing, Robotics and Computer-Integrated Manufacturing, 37, 2016, 139–150. <https://doi.org/10.1016/j.rcim.2015.09.002>.



- [3] Gao, Y.; Wu, L.; Yan, D.-M.; Nan, L.: Near Support-Free Multi-Directional 3D Printing via Global-Optimal Decomposition, Graphical Models, 104, 2019, 101034. <https://doi.org/10.1016/j.gmod.2019.101034>.
- [4] Kanakanala, D.; Swathi, R.; Ruan, J.; Frank, L. X.; Frank, L.: A Multi-Axis Slicing Method for Direct Laser Deposition Process, Proceedings of the ASME Design Engineering Technical Conference, 1(PARTS A AND B), 2010, 425–432. <https://doi.org/10.1115/DETC2010-28442>.
- [5] Lettori, J.; Raffaelli, R.; Peruzzini, M.; Pellicciari, M.: A Framework for Hybrid Manufacturing in Robotic Cells, Computer-Aided Design & Applications, 19(5), 2022, 1029–1041. <https://doi.org/10.14733/cadaps.2022.1029-1041>.
- [6] Li, Y.; Tang, K.; He, D.; Wang, X.: Multi-Axis Support-Free Printing of Freeform Parts with Lattice Infill Structures, Computer-Aided Design, 133, 2021, 102986. <https://doi.org/10.1016/j.cad.2020.102986>.
- [7] Liu, B.; Shen, H.; Zhou, Z.; Jin, J.; Fu, J.: Research on Support-Free WAAM Based on Surface/Interior Separation and Surface Segmentation, Journal of Materials Processing Technology, 297, 2021, 117240. <https://doi.org/10.1016/j.jmatprotec.2021.117240>.
- [8] Lockett, H.; Ding, J.; Williams, S.; Martina, F.: Design for Wire + Arc Additive Manufacture: Design Rules and Build Orientation Selection, Journal of Engineering Design, 28(7–9), 2017, 568–598. <https://doi.org/10.1080/09544828.2017.1365826>.
- [9] Luo, L.; Baran, I.; Rusinkiewicz, S.; Matusik, W.: Chopper: Partitioning Models into 3D-Printable Parts, ACM Transactions on Graphics, 31(6), 2012, 1–9. <https://doi.org/10.1145/2366145.2366148>.
- [10] Marzeh, Z.; Tahmasbi, M.; Mirehi, N.: Algorithm for Finding the Largest Inscribed Rectangle in Polygon, 3(1), 2019, 29–41. <https://doi.org/10.22059/JAC.2019.71280>.
- [11] Murtezaoglu, Y.; Plakhotnik, D.; Stautner, M.; Vaneker, T.; van Houten, F. J. A. M.: Geometry-Based Process Planning for Multi-Axis Support-Free Additive Manufacturing, Procedia CIRP, 78, 2018, 73–78. <https://doi.org/10.1016/j.procir.2018.08.175>.
- [12] Rauch, M.; Hascoet, J.-Y.; Querard, V.: A Multiaxis Tool Path Generation Approach for Thin Wall Structures Made with WAAM, Journal of Manufacturing and Materials Processing, 5(4), 2021, 128. <https://doi.org/10.3390/jmmp5040128>.
- [13] Ren, L.; Sparks, T.; Ruan, J.; Liou, F.: Process Planning Strategies for Solid Freeform Fabrication of Metal Parts, Journal of Manufacturing Systems, 27(4), 2008, 158–165. <https://doi.org/10.1016/j.jmsy.2009.02.002>.
- [14] Ruan, J.; Sparks, T. E.; Panackal, A.; Liou, F. W.; Eiamsa-Ard, K.; Slattery, K.; Chou, H. N.; Kinsella, M.: Automated Slicing for a Multiaxis Metal Deposition System, Journal of Manufacturing Science and Engineering, Transactions of the ASME, 129(2), 2007, 303–310. <https://doi.org/10.1115/1.2673492>.
- [15] Saboori, A.; Gallo, D.; Biamino, S.; Fino, P.; Lombardi, M.: An Overview of Additive Manufacturing of Titanium Components by Directed Energy Deposition: Microstructure and Mechanical Properties, Applied Sciences (Switzerland), 7(9), 2017, 883. <https://doi.org/10.3390/app7090883>.
- [16] Singh, P.; Dutta, D.: Multi-Direction Slicing for Layered Manufacturing, Journal of Computing and Information Science in Engineering, 1(2), 2001, 129–142. <https://doi.org/10.1115/1.1375816>.
- [17] Strong, D.; Kay, M.; Conner, B.; Wakefield, T.; Manogharan, G.: Hybrid Manufacturing – Integrating Traditional Manufacturers with Additive Manufacturing (AM) Supply Chain, Additive Manufacturing, 21, 2018, 159–173. <https://doi.org/10.1016/j.addma.2018.03.010>.
- [18] Tagliasacchi, A.; Delame, T.; Spagnuolo, M.; Amenta, N.: 3D Skeletons: A State-of-the-Art Report, Computer Graphics Forum, 35(2), 2016, 573–597.
- [19] Urhal, P.; Weightman, A.; Diver, C.; Bartolo, P.: Robot Assisted Additive Manufacturing: A Review, Robotics and Computer-Integrated Manufacturing, 59, 2019, 335–345. <https://doi.org/10.1016/j.rcim.2019.05.005>.
- [20] Wang, X.; Chen, L.; Lau, T.-Y.; Tang, K.: A Skeleton-Based Process Planning Framework for Support-Free 3+2-Axis Printing of Multi-Branch Freeform Parts, The International Journal of

- Advanced Manufacturing Technology, 110(1-2), 2020, 327-350. <https://doi.org/10.1007/s00170-020-05790-0>.
- [21] Wei, X.; Qiu, S.; Zhu, L.; Feng, R.; Tian, Y.; Xi, J.; Zheng, Y.: Toward Support-Free 3D Printing: A Skeletal Approach for Partitioning Models, IEEE Transactions on Visualization and Computer Graphics, 24(10), 2018, 2799-2812. <https://doi.org/10.1109/TVCG.2017.2767047>.
- [22] Williams, S. W.; Martina, F.; Addison, A. C.; Ding, J.; Pardal, G.; Colegrove, P.: Wire + Arc Additive Manufacturing, Materials Science and Technology (United Kingdom), 32(7), 2016, 641-647. <https://doi.org/10.1179/1743284715Y.0000000073>.
- [23] Williams, S. W.; Martina, F.; Addison, A. C.; Ding, J.; Pardal, G.; Colegrove, P.; Number, D.; Waammat, S. W. W.; Oct, A.; Williams, S. W.; Martina, F.; Williams, S. W.: Wire+arc Additive Manufacturing vs. Traditional Machining from Solid: A Cost Comparison, Materials Science and Technology (United Kingdom), 32(October), 2015, 27.
- [24] Wu, C.; Dai, C.; Fang, G.; Liu, Y. J.; Wang, C. C. L.: General Support-Effective Decomposition for Multi-Directional 3-D Printing, IEEE Transactions on Automation Science and Engineering, 17(2), 2020, 599-610. <https://doi.org/10.1109/TASE.2019.2938219>.
- [25] Xiao, X.; Joshi, S.: Process Planning for Five-Axis Support Free Additive Manufacturing, Additive Manufacturing, 36, 2020, 101569. <https://doi.org/10.1016/j.addma.2020.101569>.
- [26] Xie, F.; Jing, X.; Zhang, C.; Chen, S.; Bi, D.; Li, Z.; He, D.; Tang, K.: Volume Decomposition for Multi-Axis Support-Free and Gouging-Free Printing Based on Ellipsoidal Slicing, Computer-Aided Design, 143, 2022, 103135. <https://doi.org/10.1016/j.cad.2021.103135>.
- [27] Xu, J.; Gu, X.; Ding, D.; Pan, Z.; Chen, K.: A Review of Slicing Methods for Directed Energy Deposition Based Additive Manufacturing, Rapid Prototyping Journal, 24(6), 2018, 1012-1025. <https://doi.org/10.1108/RPJ-10-2017-0196>.
- [28] Xu, K.; Chen, L.; Tang, K.: Support-Free Layered Process Planning Toward 3 + 2-Axis Additive Manufacturing, IEEE Transactions on Automation Science and Engineering, 16(2), 2019, 838-850. <https://doi.org/10.1109/TASE.2018.2867230>.
- [29] Zhang, J.; Liou, F.: Adaptive Slicing for a Multi-Axis Laser Aided Manufacturing Process, Journal of Mechanical Design, 126(2), 2004, 254-261. <https://doi.org/10.1115/1.1649966>.
- [30] Zhao, G.; Ma, G.; Feng, J.; Xiao, W.: Nonplanar Slicing and Path Generation Methods for Robotic Additive Manufacturing, International Journal of Advanced Manufacturing Technology, 96(9-12), 2018, 3149-3159. <https://doi.org/10.1007/s00170-018-1772-9>.
- [31] WAAM3D, <https://waam3d.com/>.